International Journal of Thermophysics, Vol. 24, No. 6, November 2003 (© 2003)

Thermodynamic Properties of Gaseous Nitrous Oxide and Nitric Oxide From Speed-of-Sound Measurements

J. J. Hurly[1]

Received September 2, 2003

The speed of sound was measured in gaseous nitrous oxide (N_2O) and nitric oxide (NO) using an acoustic resonance technique with a relative standard uncertainty of less than 0.01%. The measurements span the temperature range 200 to 460 K at pressures up to the lesser of 1.6 MPa or 80% of the vapor pressure. The data were analyzed to obtain the constant-pressure ideal-gas heat capacity C_p^0 as a function of temperature with a relative standard uncertainty of 0.1%. For N_2O, the values of C_p^0 agree within 0.1% with those determined from spectroscopic data. For NO, the values of C_p^0 differ from spectroscopic results by as much as 1.5%, which is slightly more than the combined uncertainties. The speed-of-sound data were fitted by virial equations of state to obtain temperature-dependent density virial coefficients. Two virial coefficient models were employed, one based on square-well intermolecular potentials, and the second based on a hard-core Lennard-Jones intermolecular potential. The resulting virial equations reproduced nearly all the sound-speed data to within $\pm 0.01\%$ and may be used to calculate vapor densities with relative standard uncertainties of 0.1% or less.

KEY WORDS: equation of state; ideal-gas heat capacity; intermolecular potential; nitric oxide; nitrous oxide; NO; N_2O; speed of sound; thermodynamic properties; virial coefficients.

1. INTRODUCTION

Measurements of the speed of sound $u(T, p)$ in gaseous nitrous oxide (N_2O, $N{\equiv}N{=}O$) and nitric oxide (NO, $N{\equiv}O$) are reported as a function of the temperature T and pressure p. The data span the temperature range 200 to 460 K at pressures up to the lesser of 1.6 MPa or 80% of the vapor

[1] Process Measurements Division, Chemical Science and Technology Laboratory, National Institute of Standards and Technology, Gaithersburg, Maryland 20899-8360, U.S.A. E-mail: john.hurly@nist.gov

0195-928X/03/1100-1611/0 © 2003 Plenum Publishing Corporation

pressure. The measurements were made in a cylindrical cavity using a highly precise acoustic resonance technique. The speed-of-sound results typically have relative uncertainties of $0.0001 \times u$. The data were collected along isotherms. The constant-pressure ideal-gas heat capacity $C_p^0(T)$ was determined for each isotherm with an uncertainty of $0.001 \times C_p^0(T)$. The second $B(T)$ and third $C(T)$ virial coefficients were deduced for each species from fitting model intermolecular potentials to the entire $u(T, p)$ surface. The densities $\rho(T, p)$ calculated from the virial equations of state have estimated uncertainties of less than $0.001 \times \rho$ [1] for the conditions spanned by the measurements.

Both nitrous oxide and nitric oxide are used in semiconductor processing as a source of nitrogen for the growth of nitrided silicon oxide, silicon nitride, and oxynitride films on silicon surfaces by annealing in a nitrogen-rich environment. Both molecules also play important roles in medical and environmental sciences. Nitric oxide is a colorless, nonflammable, toxic gas with a slight odor, and its critical parameters are $T_c = 180.15$ K, $p_c = 6.48$ MPa, and $V_c = 0.058$ m$^3 \cdot$ kmol [2]. Nitrous oxide is a colorless, nontoxic, nonflammable gas with a slightly sweet taste and odor, and the critical parameters are $T_c = 309.57$ K, $p_c = 7.245$ MPa, and $V_c = 0.0974$ m$^3 \cdot$ kmol [2].

The speed-of-sound measurements reported in this manuscript were obtained using an apparatus and experimental methods which have a documented history of accuracy and reliability. The apparatus [3] and the acoustic model [4, 5] used to analyze the data are described in previous publications. Measurements have previously been reported for gases such as chlorine [6], nitrogen trifluoride, ethylene oxide, trimethyl gallium [7], hydrogen bromide, boron trichloride [8], and tungsten hexafluoride [9]. Detailed descriptions of the experimental technique can be found in these references.

2. NITROUS OXIDE

The speed of sound was measured in nitrous oxide at 313 states along 13 isotherms between 220 and 460 K at pressures up to 1.5 MPa or 80% of the vapor pressure [10]. All measurements are above the triple point temperature of N_2O which is approximately 182.3 K [11]. The manufacturer of the gas specified that the sample was VSLI (very large-scale integration) grade, 99.999% by mass fraction. When drawn from the source bottle, no over-pressure was observed at liquid nitrogen temperatures (≈ 77 K). The resonator was filled three times directly from the source bottle to 1.0 MPa, at 300 K. Each time the resonance frequency of the (3, 0, 0) mode was measured, and was reproduced to within 10 ppm in frequency

f or $0.00001 \times f$. The (3, 0, 0) mode is the third longitudinal mode of our cylindrical resonator using the notation of Gillis [4]. This demonstrated that a gas of constant composition was being delivered. A fresh aliquot of N_2O gas was taken from the source bottle for each isotherm. At the low-pressure end of each isotherm, the resonance frequencies were monitored for four hours while holding the temperature and pressure constant. Again, the measured frequencies all agreed to $0.00001 \times f$ indicating that the gas composition did not change while the gas was in the resonator.

At each temperature and pressure, the resonance frequency was measured at the third and fourth longitudinal modes and the first radial mode. The acoustic model for a cylindrical resonator [4] was then used to determine the speed of sound from the resonance frequencies. The model requires the cylinder's dimensions, and values for the viscosity and thermal conductivity of the gas to accurately account for bulk and surface losses. The dimensions are determined by calibration with argon, a gas for which the speed of sound is accurately known. The molar mass weight of NO was taken as $m = 44.013\ \mathrm{g \cdot mol^{-1}}$. Experimental transport property data are not available for NO, so values were predicted using a corresponding states model [12, 13].

The results for $u(T, p)$ for N_2O are listed in Table I. At each T and p, the three values of $u(T, p)$ determined from the three modes were averaged, weighted by the standard deviation of their fit to the acoustic model. The weighted mean of the three values of $u(T, p)$ and the relative standard deviation $\sigma[u]/u \times 10^6$ with a coverage factor of $k = 1$ are listed in Table I.

3. NITRIC OXIDE

The speed of sound was measured in nitric oxide at 162 states along 14 isotherms between 200 and 440 K, at pressures up to 1.4 MPa. The vapor pressure [14] was never approached since the critical temperature for NO is $T_c = 180.15$ K [2], and the triple point temperature is approximately 109.51 K [11]. At each temperature and pressure, the resonance frequency was measured at the third and fourth longitudinal modes and the first radial mode. The acoustic model for a cylindrical resonator [4] was then used to determine the speed of sound from resonance frequencies. The model requires values for the viscosity [15] and thermal conductivity [16] of the gas to accurately account for bulk and surface losses. The molar mass, m is $30.0061\ \mathrm{g \cdot mol^{-1}}$.

The three values of $u(T, p)$ were averaged, weighted by the standard fractional deviation from the fit of the acoustic model. These weighted mean values of $u(T, p)$ for NO are listed in Table II, along with their relative standard deviation $\sigma[u]/u \times 10^6$ with a coverage factor of $k = 1$.

Table I. Measured Speed of Sound of Nitrous Oxide, N_2O

P (kPa)	u (m·s^{-1})	$\sigma \times 10^6$	P (kPa)	u (m·s^{-1})	$\sigma \times 10^6$	P (kPa)	u (m·s^{-1})	$\sigma \times 10^6$
				$T = 220$ K				
491.7	223.280	66.2	354.6	226.435	66.2	201.3	229.753	56.8
457.8	224.084	82.8	300.9	227.620	57.2	152.8	230.764	50.3
403.2	225.343	71.0	254.5	228.630	52.8			
				$T = 240$ K				
988.3	225.655	89.9	615.6	232.849	51.4	323.3	237.916	60.8
898.4	227.481	85.2	555.1	233.932	50.3	278.8	238.650	42.0
831.5	228.806	72.3	510.6	234.717	48.0	235.4	239.360	104.2
784.0	229.721	66.3	459.6	235.603	50.9	192.3	240.064	85.3
724.2	230.851	65.4	413.5	236.393	46.2	146.5	240.785	96.5
695.7	231.384	56.0	372.0	237.097	40.2	98.9	241.540	94.8
				$T = 260$ K				
1642.1	228.020	40.7	1052.8	237.602	26.7	500.7	245.462	62.8
1578.8	229.127	50.2	1009.6	238.247	26.7	455.2	246.073	63.5
1519.6	230.145	45.2	928.0	239.456	37.6	413.0	246.636	59.0
1465.0	231.066	47.1	887.0	240.056	45.9	356.8	247.379	60.4
1413.0	231.930	40.6	810.0	241.167	47.5	323.3	247.820	62.5
1364.3	232.726	34.5	772.4	241.703	54.6	278.4	248.403	58.6
1272.2	234.205	28.2	702.8	242.684	55.6	252.0	248.747	57.9
1226.9	234.923	25.4	669.3	243.152	57.3	185.9	249.599	62.7
1181.6	235.629	23.1	607.4	244.007	57.2	145.0	250.119	64.3
1095.8	236.949	24.7	550.8	244.783	62.1	102.2	250.664	68.0
				$T = 280$ K				
1555.4	243.107	30.5	1050.5	249.143	60.1	500.9	255.238	39.6
1517.7	243.581	12.5	998.6	249.734	74.0	457.2	255.706	39.9
1480.9	244.034	21.9	948.4	250.303	68.2	417.3	256.132	44.2
1412.0	244.869	17.7	900.2	250.853	69.5	367.4	256.658	38.8
1377.5	245.291	24.7	831.4	251.623	63.8	321.9	257.138	38.2
1312.8	246.066	38.0	786.6	252.121	69.1	277.3	257.605	43.4
1251.0	246.801	39.7	721.4	252.837	59.2	232.9	258.068	56.6
1219.8	247.169	44.4	658.2	253.536	54.3	189.1	258.527	46.6
1161.3	247.857	55.1	617.4	253.978	52.1	147.3	258.963	51.1
1104.8	248.511	59.0	547.8	254.734	50.2	100.7	259.439	48.8
				$T = 300$ K				
1608.7	254.318	62.1	1105.0	259.033	48.7	484.7	264.560	40.2
1615.3	254.260	62.2	994.9	260.035	45.9	435.2	264.989	42.2
1545.6	254.923	70.4	941.8	260.512	45.5	389.9	265.380	40.9
1477.4	255.572	69.4	891.9	260.962	40.5	331.4	265.882	36.0
1411.9	256.191	56.9	798.4	261.802	37.3	266.8	266.436	42.2
1347.7	256.789	61.3	755.1	262.183	35.3	214.3	266.886	42.7

Table I. *(Continued)*

P (kPa)	u (m·s^{-1})	$\sigma \times 10^6$	P (kPa)	u (m·s^{-1})	$\sigma \times 10^6$	P (kPa)	u (m·s^{-1})	$\sigma \times 10^6$
				$T = 300$ K				
1285.5	257.367	58.3	676.0	262.885	37.7	153.7	267.403	42.3
1223.7	257.940	54.5	603.9	263.518	35.7	99.2	267.867	31.6
1163.1	258.498	47.5	540.3	264.078	38.0			
				$T = 320$ K				
1604.1	264.993	142.5	992.1	269.538	46.1	454.0	273.426	23.4
1566.2	265.274	81.3	945.1	269.881	40.9	411.5	273.732	31.8
1493.3	265.822	83.1	900.2	270.209	30.5	372.9	274.008	38.8
1458.0	266.087	82.5	837.0	270.667	24.8	321.6	274.373	43.0
1390.0	266.596	81.1	778.0	271.098	14.5	277.3	274.689	44.3
1325.0	267.081	77.4	723.2	271.493	7.6	233.3	275.005	41.2
1293.5	267.315	77.4	672.1	271.861	10.0	191.4	275.303	57.1
1232.9	267.767	70.1	609.5	272.313	7.4	145.9	275.628	58.8
1174.9	268.194	66.4	552.6	272.721	13.0	100.7	275.956	58.3
1119.6	268.603	57.4	500.9	273.091	20.4	100.7	275.951	55.7
1066.7	268.992	53.4						
				$T = 340$ K				
1634.4	274.611	131.0	1056.5	278.101	45.9	498.4	281.429	26.2
1593.0	274.865	125.6	953.1	278.724	36.4	449.2	281.724	31.5
1513.7	275.346	113.1	905.0	279.009	33.4	384.2	282.106	33.9
1438.1	275.803	104.7	837.4	279.412	22.8	328.6	282.438	36.6
1331.8	276.445	87.8	755.1	279.904	15.2	273.9	282.765	50.2
1265.2	276.846	81.8	698.6	280.240	8.0	216.7	283.105	39.6
1201.7	277.231	65.6	629.7	280.650	20.9	158.5	283.453	52.5
1112.5	277.766	57.0	553.1	281.106	24.6	101.9	283.797	50.1
				$T = 360$ K				
1624.2	283.859	98.6	1019.6	286.849	37.5	499.7	289.419	41.1
1580.3	284.072	101.3	939.2	287.249	34.7	447.7	289.675	38.5
1496.1	284.495	92.4	889.0	287.496	33.9	390.3	289.962	39.0
1416.4	284.887	81.9	818.8	287.839	28.9	331.1	290.253	41.6
1340.9	285.260	68.7	754.0	288.162	26.0	273.4	290.541	51.5
1269.4	285.614	59.6	675.7	288.547	28.4	213.6	290.841	53.7
1169.4	286.109	53.9	622.3	288.814	27.2	158.1	291.117	58.2
1107.0	286.417	45.1	557.6	289.131	31.4	102.2	291.400	69.7
				$T = 380$ K				
1593.6	292.654	112.9	1060.8	294.827	66.2	561.2	296.880	55.4
1593.6	292.654	112.9	1001.1	295.068	69.6	500.0	297.131	53.9
1547.8	292.841	117.5	944.6	295.300	62.0	458.5	297.305	47.8
1460.3	293.194	107.4	891.4	295.526	73.7	396.9	297.559	56.1
1418.2	293.365	93.7	841.2	295.726	60.8	353.7	297.741	65.1
1338.2	293.692	96.7	771.3	296.015	65.5	297.5	297.974	54.5

Table I. *(Continued)*

P (kPa)	u (m·s^{-1})	$\sigma \times 10^6$	P (kPa)	u (m·s^{-1})	$\sigma \times 10^6$	P (kPa)	u (m·s^{-1})	$\sigma \times 10^6$
				$T = 380$ K				
1262.7	293.997	80.7	727.9	296.192	59.3	250.4	298.165	67.9
1191.4	294.296	82.5	667.4	296.443	53.3	198.9	298.391	54.6
1124.2	294.567	70.0	612.0	296.669	50.5	149.4	298.599	83.7
				$T = 400$ K				
1623.8	300.777	118.5	997.0	302.888	73.1	560.5	304.381	54.9
1527.3	301.097	115.9	938.2	303.085	73.1	427.2	304.844	61.8
1436.6	301.400	109.1	856.5	303.366	64.5	378.7	305.013	65.8
1311.0	301.827	100.1	758.7	303.700	53.9	263.9	305.418	61.7
1196.6	302.211	95.6	692.7	303.926	62.4	178.7	305.720	66.5
1092.2	302.562	76.2	595.5	304.262	54.4	168.3	305.758	64.6
				$T = 420$ K				
1618.4	308.684	112.3	1032.1	310.311	72.5	546.9	311.692	54.9
1566.8	308.823	126.0	968.3	310.486	72.3	482.1	311.878	56.9
1469.0	309.089	124.1	908.5	310.662	63.3	424.9	312.042	57.9
1422.2	309.221	109.7	852.4	310.817	64.7	363.0	312.227	58.5
1333.7	309.462	104.6	775.0	311.034	59.9	291.4	312.438	66.0
1250.7	309.698	90.8	727.3	311.171	58.8	226.8	312.633	63.0
1173.0	309.912	75.4	661.2	311.362	62.4	165.9	312.817	65.1
1100.3	310.113	84.7	601.3	311.530	54.6	100.9	313.018	83.7
				$T = 440$ K				
1643.7	316.199	116.3	1093.8	317.471	76.0	546.5	318.756	48.9
1602.4	316.312	117.3	990.1	317.707	61.5	495.2	318.882	43.8
1592.4	316.328	125.3	957.6	317.784	61.5	434.5	319.028	50.2
1581.8	316.351	123.7	896.1	317.923	65.8	381.2	319.148	60.4
1529.3	316.471	130.1	838.6	318.061	60.3	323.8	319.293	52.6
1429.8	316.693	108.7	784.9	318.186	60.6	266.3	319.447	67.2
1382.4	316.802	107.5	711.0	318.361	56.9	205.4	319.601	52.8
1292.8	317.004	104.5	665.6	318.472	50.9	148.6	319.744	74.8
1250.0	317.101	91.1	603.0	318.615	56.0	101.0	319.866	90.3
1169.2	317.291	75.3						
				$T = 460$ K				
1615.5	323.5948	183.6	1021.2	324.7127	119.1	560.8	325.6121	97.9
1558.9	323.6991	171.6	951.5	324.8472	116.7	487.9	325.7591	101.0
1452.4	323.8979	171.8	918.4	324.9069	122.1	439.7	325.8573	90.9
1401.7	323.9930	158.4	855.5	325.0323	115.9	424.6	325.8891	97.2
1306.4	324.1699	145.9	797.1	325.1451	112.5	320.8	326.1056	90.9
1261.1	324.2550	140.3	717.0	325.3002	99.7	269.5	326.2108	107.1
1175.7	324.4166	139.5	668.3	325.3983	105.8	211.2	326.3368	101.1
1095.9	324.5672	126.7	601.5	325.5318	96.8	204.0	326.3491	107.0

The NO source bottle purity was only 99.6% by mass fraction. The manufacturer reported that the impurities were NO_2 and N_2O_2. To exploit the accuracy of the speed-of-sound technique, we required either a purer sample or a better characterized sample. The toxic and reactive nature of NO made a more accurate characterization difficult. We chose to purify the sample by the following procedure. An aliquot was taken from the source bottle and transferred into a smaller bottle. The smaller bottle was placed in liquid nitrogen, cooling it to approximately 77 K. An over-pressure of a few kilopascals was observed, indicating a volatile impurity. The over-pressure was pumped away, and a series of freeze-pump-thaw cycles was repeated until no appreciable over-pressure was observed at 77 K.

The sample was then allowed to warm and was expanded into the resonator. The (3, 0, 0) resonance frequency was measured at 300 K and 500 kPa. The sample was pulled back into the source bottle at 77 K, and the process repeated. The resulting measured frequencies differed by as much as $0.0003 \times f$; however, once the sample was loaded into the resonator, the monitored resonance frequency remained constant with time to $0.00001 \times f$. This indicated that the sample composition was stable once loaded into the resonator, but an inconsistent composition was being delivered from the source bottle. If after each successive loading of the sample, the frequency shifted in a consistent direction, one could assume some reaction was occurring during the loading process. However, this was not the case; the shift in frequency was random. This is consistent with an impurity such as NO_2 or N_2O_2 that has a very low vapor pressure and is solid at 77 K. When the sample was warmed, the first (and major component) to evolve was NO, with the impurities evolving at higher temperatures in an irreproducible manner.

We took advantage of the low normal boiling point of NO, $T_{nbp} = 121.4$ K [11], compared to NO_2, $T_{nbp} = 294$ K [11] and other nitrous oxides, N_2O_x all of which have $T_{nbp} < 298.15$ K [11]. The sample of NO was collected into the source bottle at 77 K. The liquid nitrogen was then replaced with a Dewar containing a dry ice/acetone slurry ≈ 195 K. As the vapor evolved, it flowed into the resonator, at the maximum working pressure of our system, 1.5 MPa, the resonator was isolated, and the sample bottle allowed to warm to room temperature, at which point all of its contents were evacuated. The sample in the resonator was then pulled back into the source bottle at 77 K. This procedure was repeated three times, acting as a distillation in which the NO vapor was saved, but the contaminants trapped at 195 K were isolated and removed. The same procedure was used to load the resonator for each isotherm, with the exception that the source bottle was not evacuated after each loading. The sample in the manifold would have been lost, which was not a negligible volume of

Table II. Measured Speed of Sound of Nitric Oxide, NO

P (kPa)	u (m·s^{-1})	$\sigma \times 10^6$	P (kPa)	u (m·s^{-1})	$\sigma \times 10^6$	P (kPa)	u (m·s^{-1})	$\sigma \times 10^6$
				$T = 200$ K				
693.3	272.015	57	398.9	273.412	36	214.4	274.289	13
592.3	272.493	53	340.5	273.687	29	148.2	274.604	6
546.1	272.710	49	270.4	274.022	20	96.8	274.847	3
467.0	273.085	40						
				$T = 220$ K				
761.5	286.819	65	443.8	287.811	33	226.6	288.495	6
661.9	287.130	51	382.3	288.004	24	157.6	288.713	7
618.5	287.265	38	304.4	288.247	10	76.0	288.971	7
541.6	287.502	45						
				$T = 240$ K				
821.2	300.800	35	478.9	301.470	20	245.6	301.937	12
728.8	300.979	26	404.6	301.617	19	177.1	302.078	16
669.8	301.094	28	342.4	301.743	16	95.9	302.237	17
568.2	301.290	18						
				$T = 250$ K				
853.1	307.554	27	482.2	308.113	8	239.0	308.498	15
727.5	307.741	10	411.0	308.226	10	164.1	308.619	16
670.6	307.824	4	326.0	308.359	16	74.7	308.762	20
567.1	307.983	10						
				$T = 260$ K				
882.6	314.139	11	521.0	314.549	14	271.2	314.848	28
793.7	314.237	7	442.3	314.639	17	180.6	314.958	29
670.0	314.376	8	345.9	314.756	23	99.7	315.059	33
616.7	314.438	9						
				$T = 280$ K				
950.4	326.839	34	682.8	326.973	39	329.1	327.169	41
949.8	326.841	34	628.5	327.001	43	260.1	327.210	46
947.6	326.842	37	534.0	327.055	39	176.1	327.264	42
874.0	326.875	41	491.6	327.076	43	97.9	327.312	41
803.8	326.913	38	418.6	327.116	41			
				$T = 300$ K				
1007.6	339.134	34	696.1	339.135	16	402.6	339.157	29
917.9	339.134	31	634.8	339.137	19	281.3	339.164	42
837.2	339.128	27	579.0	339.146	13	198.0	339.184	38
762.0	339.129	27	483.3	339.147	35	100.5	339.188	52

Table II. *(Continued)*

P (kPa)	u (m·s^{-1})	$\sigma \times 10^6$	P (kPa)	u (m·s^{-1})	$\sigma \times 10^6$	P (kPa)	u (m·s^{-1})	$\sigma \times 10^6$
				$T = 320$ K				
1075.8	350.718	38	643.0	350.571	44	319.3	350.481	55
970.8	350.683	40	524.9	350.536	43	194.8	350.452	61
873.3	350.647	41	429.4	350.510	50	98.7	350.432	73
712.1	350.596	32						
				$T = 340$ K				
1120.5	361.961	80	717.3	361.707	34	373.7	361.506	45
1002.2	361.888	58	643.4	361.660	38	301.7	361.466	60
895.9	361.817	51	575.9	361.620	33	198.2	361.414	63
802.2	361.761	42	464.8	361.554	37	99.3	361.357	82
				$T = 360$ K				
1184.0	372.878	55	762.2	372.502	45	402.1	372.202	69
1060.9	372.769	45	615.8	372.382	49	293.8	372.118	81
949.9	372.668	44	553.1	372.325	55	194.9	372.041	85
849.8	372.577	51	497.0	372.283	61	98.2	371.982	38
				$T = 380$ K				
1235.0	383.389	69	720.5	382.845	37	380.9	382.481	83
1110.6	383.254	56	647.5	382.761	57	308.9	382.424	72
996.4	383.125	65	581.4	382.695	71	186.6	382.299	94
894.9	383.011	98	470.5	382.570	130	94.8	382.235	19
				$T = 400$ K				
1276.8	393.531	62	793.9	392.940	56	394.8	392.471	82
1132.4	393.353	60	629.0	392.742	70	314.4	392.377	88
1004.2	393.196	57	560.1	392.660	72	223.9	392.276	95
1003.1	393.191	62	497.9	392.589	71	143.8	392.187	90
892.2	393.058	52						
				$T = 420$ K				
1331.9	403.383	77	811.9	402.682	68	394.0	402.136	92
1178.8	403.175	84	719.1	402.558	71	311.4	402.032	100
1039.0	402.986	67	637.7	402.450	71	220.0	401.919	108
1037.7	402.981	78	564.7	402.358	78	139.9	401.816	119
917.1	402.821	68	500.4	402.273	92			
				$T = 440$ K				
1386.3	412.944	50	828.8	412.130	87	393.8	411.510	125
1218.4	412.712	56	730.7	411.990	104	308.3	411.386	130
1070.9	412.489	67	644.3	411.862	100	242.0	411.293	134
1069.5	412.485	66	569.4	411.757	110	151.2	411.166	145
941.5	412.296	82	501.9	411.655	110			

gas. Using this loading procedure, a consistent composition sample was delivered to the resonator as indicated by the same resonance frequency being measured to $0.00001 \times f$ after three successive loadings to the same T and p. We point out that the sample delivered to the resonator was consistent in composition; however, its absolute purity was not known.

After all measurements were completed, the sample was allowed to warm to room temperature and was analyzed with a gas chromatograph. The sample was found to be 99.98% pure with a 0.02% unknown by peak area ratio. The unknown came off the column earlier than the main peak. A portion of the NO could have reacted in the column to create the 0.02%, or the 0.02% could have been in the sample which was studied. If the impurity were 0.02% N_2O_2 by mole fraction, then the mean molar mass of the sample would be 0.02% higher than $30.0061\ \mathrm{gm \cdot mol^{-1}}$ resulting in a decrease in the calculated heat capacity of less than 0.07%. The effect of 0.02% N_2O_2 (by mole fraction) on the equation of state would be insignificant.

4. IDEAL-GAS HEAT CAPACITY, $C_p^0(T)$

The speed-of-sound data were collected along isotherms. The acoustic virial equation of state was fit to the data on each isotherm. The acoustic virial equation of state is

$$u^2 = \frac{\gamma^0 RT}{m}\left(1 + \frac{\beta_a p}{RT} + \frac{\gamma_a p^2}{RT} + \frac{\delta_a p^3}{RT} + \cdots\right) \tag{1}$$

where m is the molar mass, $R = 8.314472\ \mathrm{J \cdot mol^{-1} \cdot K^{-1}}$ [17] is the universal molar gas constant, T is the temperature in K (ITS-90), C_p^0 is the constant-pressure ideal-gas heat capacity, $\gamma^0 = C_p^0/C_v^0$ is the zero-pressure limit of the heat-capacity ratio, and β_a, γ_a, and δ_a are the temperature-dependent acoustic virial coefficients. The constant-pressure ideal-gas heat capacity C_p^0 was obtained from the fit of Eq. (1) through the relation $C_p^0/R = \gamma^0/(\gamma^0 - 1)$.

Table III lists the resulting values for $C_p^0(T)$, β_a, γ_a, and δ_a for N_2O and NO. Also listed are the statistical uncertainties of each value from the fitting. These uncertainties do not include contributions from possible impurities; they are just a measure of the goodness of the fit.

The constant-volume ideal-gas heat capacity C_v^0 is the sum of the translational ($C_{v,\mathrm{tr}}^0$), rotational ($C_{v,\mathrm{rot}}^0$), and vibrational ($C_{v,\mathrm{vib}}^0$) components and, in some special cases, the electronic ($C_{v,\mathrm{el}}^0$) component.

$$C_v^0 = C_{v,\mathrm{tr}}^0 + C_{v,\mathrm{rot}}^0 + C_{v,\mathrm{vib}}^0 + C_{v,\mathrm{el}}^0 \tag{2}$$

Table III. Ideal-Gas Heat Capacity at Constant Pressure and Acoustic Virial Coefficients Obtained from Fitting Each Isotherm to the Acoustic Virial Equation of State, Eq. (1)

T (K)	$C_p^0(T)$ (R)	$\beta_a(T)$ ($cm^3 \cdot mol^{-1}$)	$\gamma_a(T)$ ($cm^6 \cdot mol^{-2}$)	$\delta_a(T)$ ($cm^6 \cdot mol^{-2}$)
		Nitrous Oxide (N_2O)		
220	4.168±0.0040	−307.20±5.90	−31.83±20.16	−22.36±21.09
240	4.296±0.0008	−254.71±0.68	−13.89±1.39	−11.06±0.85
260	4.419±0.0004	−215.48±0.27	−6.66±0.33	−4.37±0.12
280	4.538±0.0004	−182.27±0.28	−4.52±0.36	−1.46±0.14
300	4.650±0.0002	−156.13±0.17	−2.51±0.24	−0.53±0.10
320	4.756±0.0003	−136.80±0.17	1.43±0.25	−1.02±0.10
340	4.857±0.0003	−118.86±0.24	2.58±0.35	−0.91±0.15
360	4.953±0.0003	−102.87±0.23	2.62±0.31	−0.63±0.12
380	5.044±0.0005	−89.40±0.35	2.89±0.46	−0.54±0.18
400	5.131±0.0003	−78.16±0.23	3.67±0.31	−0.67±0.12
420	5.214±0.0005	−68.72±0.37	4.86±0.50	−1.01±0.20
440	5.293±0.0007	−60.00±0.51	5.62±0.68	−1.27±0.27
460	5.363±0.0005	−54.93±0.50	8.97±0.77	−2.40±0.32
		Nitric Oxide (NO)		
200	3.720±0.00007	−57.32±0.12	0.34±0.21	
220	3.687±0.00008	−40.20±0.11	0.77±0.19	
240	3.664±0.00017	−27.02±0.19	0.94±0.22	
250	3.650±0.00014	−22.27±0.14	1.47±0.15	
260	3.639±0.00013	−17.47±0.10	1.40±0.09	
280	3.622±0.00007	−9.22±0.07	1.32±0.06	
300	3.611±0.00036	−2.40±0.32	1.25±0.26	
320	3.599±0.00015	3.06±0.14	1.22±0.11	
340	3.593±0.00017	7.76±0.18	1.26±0.14	
360	3.587±0.00016	11.23±0.19	1.69±0.15	
380	3.585±0.00041	14.72±0.49	1.70±0.36	
400	3.587±0.00014	18.67±0.14	1.09±0.09	
420	3.590±0.00009	21.48±0.09	0.98±0.06	
440	3.597±0.00039	25.26±0.39	0.39±0.22	

At the temperatures in the present work, the rotational mode is fully excited so that $C^0_{v,tr} + C^0_{v,rot} = 2.5$ R. The vibrational contribution is a sum over all normal modes of vibration frequency v_i, where i is the mode number. The number of normal modes n_i for linear molecules such as NO and N_2O is given by $n_i = 3n-5$, where n is the number of atoms. Thus, NO has one vibrational mode and N_2O has four. The characteristic temperature of vibration is $\Theta_i = hv_i/k_B$, so $C^0_{v,vib}$ is given by

$$\frac{C^0_{v,vib}}{R} = \sum_{i=1}^{n_v} (\Theta_i/T)^2 \frac{\exp(\Theta_i/kT)}{[\exp(\Theta_i/kT)-1]^2} \tag{3}$$

Equation (3) is an approximation, that ignores anharmonicity and rotational-vibrational interactions. For a few diatomic molecules, notably O_2 and NO, there is an additional electronic ($C^0_{v,el}$) contribution to the specific heat resulting from two electronic levels lying close together. Oxygen has two distinct electronic energy levels separated by only 0.97 eV. Nitric oxide has a ground state that is part of a multiplet with the lowest energy gap separated by only $\varepsilon = 0.015$ eV ($\varepsilon = \varepsilon_1 - \varepsilon_2$). The degeneracy of each state is two, so the ratio of the degeneracies $\omega = \omega_2/\omega_1$ is one. For NO the electronic contribution to the specific heat is given by

$$\frac{C^0_{v,el}}{R} = (\varepsilon/kT)^2 \frac{\omega \exp(\varepsilon/kT)}{[1+\omega \exp(\varepsilon/kT)]^2} \tag{4}$$

This contribution results in a peak in the specific heat at 74 K (5000 K for O_2).

Nitrous oxide has four normal vibrational modes (two of which are degenerate) $\Theta_1 = 1836.6$ K, $\Theta_2 = \Theta_3 = 847.7$ K, and $\Theta_4 = 3199.4$ K [18]. Using Eq. (2), the three vibrational characteristic temperatures were fit to the heat capacities reported in Table III after subtracting 2.5 R to account for $C^0_{v,tr}$ and $C^0_{v,rot}$. The results of the fit were $\Theta_1 = 1839.7$ K, $\Theta_2 = \Theta_3 = 850.8$ K, and $\Theta_4 = 3149.24$ K. Equation (3) with these three parameters represents the experimental heat capacities in Table III with a standard relative uncertainty of 0.025%, and it also extrapolates well to temperatures above the experimental temperature range.

Nitric oxide has only one normal vibrational mode with a characteristic temperature of $\Theta_v = 2738.8$ K [18, 19]. However, NO also has a electronic mode as mentioned above, with a characteristic temperature of $\Theta_{el} = \varepsilon/k = 174.24$ K. Equation (2) now includes Eqs. (3) and (4), again with $C^0_{v,tr} + C^0_{v,rot} = 2.5$ R. Fitting this two-parameter equation to the C^0_p results for NO in Table III resulted in $\Theta_v = 3185.8$ K and $\Theta_{el} = 211.5$ K. This fit had a standard relative uncertainty of 0.075%. This fit reproduced our experimental values of C^0_p within their uncertainty; however, in fitting the entire speed-of-sound surface to obtain an equation of state, a slightly better fit, statistically, was used which allowed the value of $C^0_{v,tr} + C^0_{v,rot}$ to vary from its value of 2.5 R. This resulted in the values of $C^0_{v,tr} + C^0_{v,rot} = 2.474$ R, $\Theta_v = 2936.3$ K, and $\Theta_{el} = 232.54$ K. This fit only had a relative standard uncertainty of 0.02% and was used in fitting the equation of state to the speed-of-sound surface.

Figure 1 shows the results for $C^0_p(T)/R$ for each gas. The results for N_2O agree well with the values calculated from spectroscopic measurements [20–23]. The NO results show a systematic deviation. The effect of the excited electronic state are clearly observable. One-percent uncertainty

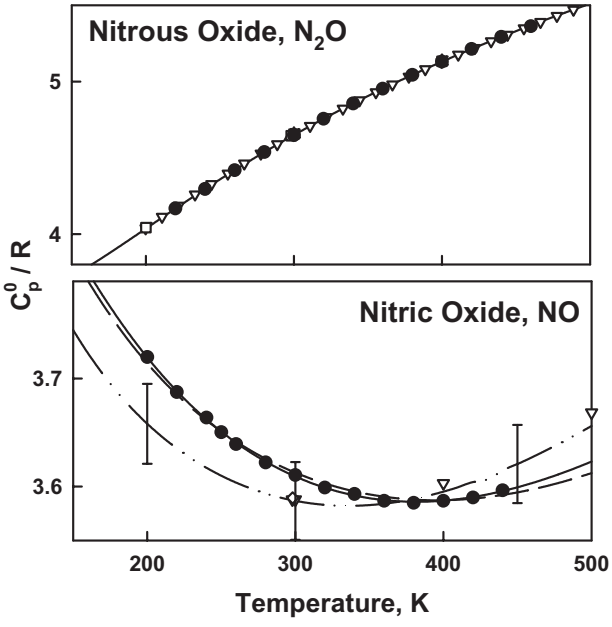

Fig. 1. Ideal-gas heat capacity at constant pressure. Nitrous oxide: (●) Present work; (——) Eq. (2) fitted to present work; (–···–) Eq. (2) from Chase, Jr. [18]; (□) Braker and Mossman [20]; (△) Westrum, Jr. et al. [21]; (▽) Touloukian [22]; (◇) Wagman et al. [23]; Nitric oxide: (– – –) three-parameter fit of Eq. (2).

bars are placed on the curve for the calculated values from Ref. 18. The present results fall within this uncertainty band, except at the lowest temperatures. The cause of the difference between our observed values of C_p^0 and those calculated from spectroscopic measurements is unclear. The difference is unlikely to result from an impurity in the gas sample. An impurity would shift the curve up or down, while Fig. 1 shows a shift to the left. Furthermore, the impurity would have to be consistently delivered during each sample loading, which is unlikely as evidenced by the internal consistency of the data set.

5. VIRIAL EQUATION OF STATE

The equation of state for a gas can be expressed in the form of a virial expansion,

$$p = RT\rho[1 + B(T)\,\rho + C(T)\,\rho^2 + \cdots] \tag{5}$$

where p is pressure, T is temperature, ρ is density, $R = 8.314472\ \mathrm{J \cdot mol^{-1} \cdot K^{-1}}$ [17] is the universal gas constant, and $B(T)$ and $C(T)$ are the second and third density virial coefficients. $B(T)$ expresses the effect of pairs of molecules interacting on the pressure of a gas, $C(T)$ describes three-body interactions, and so on. The acoustic virial coefficients in Eq. (1) are directly related to the density virial coefficients in Eq. (5) through exact thermodynamic relations involving the density virial coefficients, their temperature derivatives, and $\gamma^0(T)$ [1]. Gillis and Moldover [1] showed how Eq. (5) can be fitted directly to a $u^2(T, p)$ surface using these relationships together with a model for the density virial coefficients and their temperature dependence.

Two models for the density virial coefficients and their temperature dependence were considered, each has advantages: the hard-core square-well (HCSW) model and the hard-core Lennard-Jones (HCLJ) model. The implementation of both of these models is described in detail elsewhere [6–9]; here only the results are provided.

5.1. Hard-Core Square-Well Potential Model (HCSW)

The HCSW model is an algebraically simple representation of intermolecular interactions where the molecule has a infinitely repulsive wall at radius σ, with an attractive well of depth ε, from σ to some distance r_m, then no interactions from r_m out to infinity. This simple model has the advantage that the integral equations for the virial coefficients, which are dependent on the potential model, can be solved exactly, resulting in explicit algebraic expressions for the temperature-dependent second and third virial coefficients [1]. Given the potential parameters, the virial coefficients and their temperature derivatives can be easily calculated at any temperature. The functions also extrapolate reasonably well. These expressions are

$$\begin{aligned} B(T) &= b_0[1-(\lambda^3-1)\,\Delta] \\ C(T) &= \tfrac{1}{8} b_0^2(5-c_1\Delta-c_2\Delta^2-c_3\Delta^3) \end{aligned} \tag{6}$$

$$\begin{aligned} c_1 &= \lambda^6-18\lambda^4+32\lambda^3-15 \\ c_2 &= 2\lambda^6-36\lambda^4+32\lambda^3+18\lambda^2-16 \\ c_3 &= 6\lambda^6-18\lambda^4+18\lambda^2-6 \end{aligned} \tag{7}$$

where $\Delta = \exp \varepsilon/(k_B T) - 1$ and k_B is Boltzmann's constant. The adjustable parameters are as follows: ε is the well depth, σ is the hard-core diameter, and λ is the ratio of the width of the well to σ. Here b_0 is the molar volume of the hard core $b_0 = \frac{2}{3}\pi N_A \sigma^3$, and N_A is Avogadro's constant. Equations

(6) and (7) allow a $u^2(T, p)$ surface to be fitted directly to Eq. (5). As in Ref. 1, different values of b_0, ε, and λ were used for $B(T)$ and $C(T)$. This resulted in a model having six adjustable parameters. Equations (6) and (7) provide reasonable temperature dependences for $B(T)$ and $C(T)$; however, the fitted parameters have little physical significance. The six parameters [b_0, ε, and λ for $B(T)$ and b_0, ε, and λ for $C(T)$] in Eqs. (6) and (7) were fitted to the $u^2(T, p)$ surface for each gas, while C_p^0 was fixed at the values given by Eq. (2) with the parameters given in Section 4.

5.1.1. Nitrous Oxide, N_2O

Equation (5) was fit to the $u^2(T, p)$ surface for N_2O using the HCSW model, weighted by the σ given in Table II. The $u^2(T, p)$ data set covered sufficient densities to require the third virial coefficient. The resulting six parameters, b_0, λ, and ε/k_B for $B(T)$ and b_0, λ, and ε/k_B for $C(T)$ are given in Table VI. This six-parameter fit had 212 degrees of freedom, v, and χ^2/v was 0.71, where $\chi^2 = \sum_i [f(x_i) - f_i]^2/\sigma_f^2$; and $f(x_i) = u^2(T, p)$. Figure 2 (top) shows the fractional deviation plot of the measured speeds of sound from the HCSW equation of state. Nearly all the data are reproduced by the equation of state to within $\pm 0.01\%$.

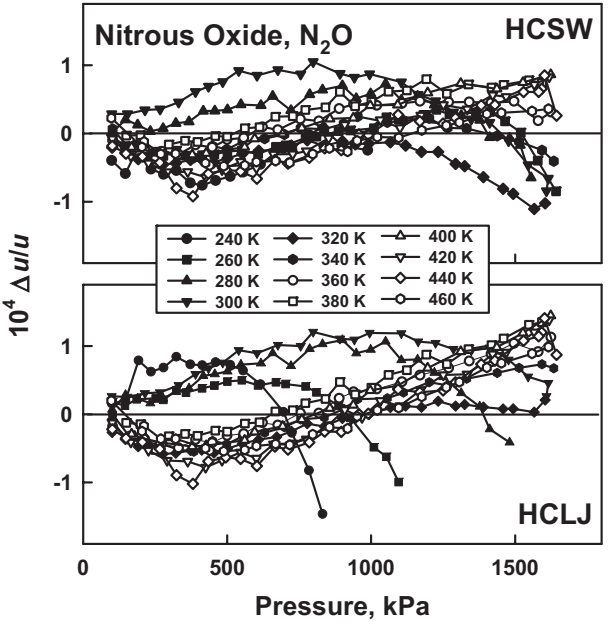

Fig. 2. Deviation plot of measured speeds of sound in N_2O from the fitted virial equations of state.

5.1.2. Nitric Oxide, NO

Equation (5) was fit to the $u^2(T, p)$ surface for NO using the HCSW model, weighted by the σ given in Table III. The $u^2(T, p)$ data set did not cover a wide enough range of densities to require a three-parameter third virial coefficient; however, a constant third virial coefficient was statistically significant. The resulting four parameters, b_0, λ, and ε/k_B for $B(T)$, and a constant for $C(T)$ are given in Table IV. This four-parameter fit had 158 degrees of freedom, v, and χ^2/v was 3.52. Figure 3 (top) shows the deviation plot of the measured speeds of sound from the HCSW equation of state. Nearly all the data are reproduced by the equation of state to within $\pm 0.01\%$. If the $u^2(T, p)$ data set was fit using the HCSW model for $C(T)$, the fitted parameters were $b_0 = 7.52231 \times 10^{-5}$ $(m^3 \cdot mol^{-1})^2$, $\lambda = 1.19268$, and $\varepsilon/k_B = 333.92$ K, and the χ^2/v was 3.26. This was not a significant improvement to justify the inclusion of two additional fitting parameters.

5.2. Hard-Core Lennard-Jones Model (HCLJ)

In this section, the square-well intermolecular potential is replaced by the more realistic hard-core Lennard-Jones 6-12 potential [24] given by

$$\varphi(r_{ij}) = 4\varepsilon \left\{ \left(\frac{\sigma - 2a}{r_{ij} - 2a} \right)^{12} - \left(\frac{\sigma - 2a}{r_{ij} - 2a} \right)^{6} \right\} \tag{8}$$

Table IV. Potential Parameters

HCSW Parameters						
	$B(T)$ $(m^3 \cdot mol^{-1})$			$C(T)$ $(m^3 \cdot mol^{-1})^2$		
	b_0 $(m^3 \cdot mol^{-1})$	λ	ε/k_B (K)	b_0 $(m^3 \cdot mol^{-1})$	λ	ε/k_B (K)
N_2O	5.2021×10^{-5}	1.4842	281.33	8.0519×10^{-5}	1.4087	294.56
NO	3.2178×10^{-5}	1.3368	226.87	1.2969×10^{-9}		

HCLJ Parameters				
	σ (nm)	a (nm)	ε/k_B (K)	v_{123}/k_B $(K \cdot nm^9)$
N_2O	0.3595	0.06281	446.77	0.005411
NO	0.3075	0.07387	323.68	0.003497

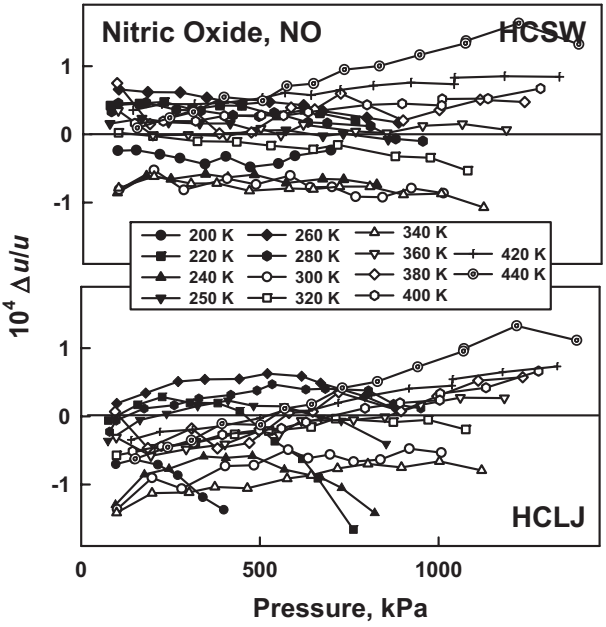

Fig. 3. Deviation plot of measured speeds of sound in NO from the fitted virial equations of state.

where r_{ij} is the intermolecular separation between molecules i and j, ε is the well depth, σ is the value of r_{ij} where $\varphi(r)$ crosses zero, and a is the radius of the hard core. This potential has three adjustable parameters: ε, σ, and a. The calculation of the third virial coefficient required the inclusion of three-body contributions. Following Trusler [25], the Axilrod–Teller triple-dipole term [26] was included which added a fourth adjustable parameter, ν_{123} to the fit.

$$\varphi(r_{123}) = \frac{\nu_{123}(1+\cos\theta_1\cos\theta_2\cos\theta_3)}{(r_{12}^3 r_{13}^3 r_{23}^3)^{-1}} \tag{9}$$

where ν_{123} is the dispersion coefficient and θ_i is defined as the angle subtended at molecule i by molecules j and k. This is the first term in the three-body corrections to the dispersion energy for monatomic species. The integral equations providing the second and third virial coefficients for spherically symmetric molecules are given by [27, 28]

$$B(T) = -2\pi N_A \int_0^\infty f_{12} r_{12}^2 \, dr_{12} \tag{10}$$

$$C(T) = -\frac{8\pi^2 N_A^2}{3} \int_0^\infty \int_0^\infty \int_{|r_{12}-r_{13}|}^{|r_{12}+r_{13}|} (f_{12} f_{13} f_{23} - e_{12} e_{13} e_{23} f_{123}) \, r_{12} r_{13} r_{23} \, dr_{12} \, dr_{13} \, dr_{23} \tag{11}$$

where N_A is Avagadro's number, r_{ij} is the distance between molecules i and j, $e_{ij} = \exp\{-\varphi(r_{ij})/(k_B T)\}$, $f_{ij} = e_{ij} - 1$, and $f_{ijk} = \exp\{-\varphi(r_{ijk})/(k_B T)\} - 1$. Equations (10) and (11) allow us to calculate the second and third virial coefficients and their temperature derivative for a given intermolecular potential at a given temperature. Equations (10) and (11) were solved using an automatic adaptive quadrature routine [29], where one can specify the desired accuracy, which was typically set to 10^{-4}. This setting was relaxed for the inner integrals in Eq. (11) during the initial fitting of Eq. (5).

The HCLJ model is a superior representation of intermolecular interactions than the HCSW model. The potential approaches infinity as the intermolecular separation approaches zero, and the potential asymptotically approaches zero at large intermolecular separations. However, both the NO and N_2O molecules are linear, not spherically symmetric. Thus, the HCLJ (and the HCSW) potentials approximate a spherical average over all collision orientations. Because the data are reproduced within their experimental uncertainties, we were not motivated to consider potentials that are anisotropic or that have a more complex shape than the HCLJ potential or a more realistic approximation to the three-body corrections to the third virial coefficient.

With $C_p^0(T)$ given by Eq. (2) and the parameters in Section 4, four potential parameters, ε, σ, a, and ν_{123} were used to fit the virial equation of state, Eq. (5), to the $u^2(T, p)$ surface for each gas. The more realistic HCLJ potential has two fewer parameters than the HCSW model with $B(T)$ and $C(T)$, and can be expected to more accurately extrapolate outside the experimental temperature range. Because the second and third virial coefficients are both calculated using the same potential parameters, the HCLJ potential is indeed a model of the intermolecular interactions in the vapor.

5.2.1. Nitrous Oxide, N_2O

Equation (5) was fit to the $u^2(T, p)$ surface for nitrous oxide using the HCLJ model. The resulting fitted four-parameters, σ, a, ε/k_B, and ν_{123}/k_B are given in Table IV. The fit had 298 degrees of freedom, ν, and χ^2/ν was 1.40. Some high-pressure (high-density) points from the isotherms below 300 K had to be excluded. Their systematic deviations showed that the fourth virial coefficient $D(T)$ was required to calculate densities at these

temperatures and pressures. The HCSW model was able to compensate by including some contribution for $D(T)$ into $B(T)$ and $C(T)$. This is because there are two additional adjustable parameters, and $B(T)$ and $C(T)$ are independent, non-coupled functions. Figure 2 (bottom) shows the deviations of the measured speeds of sound from the HCLJ equation of state for N_2O. The resulting equation of state still nearly reproduces all the speed-of-sound data to within $\pm 0.01\%$. The systematic deviations in the lower temperature isotherms in Fig. 2 (bottom) show evidence of the absence of a fourth virial contribution, and its obvious change of sign between 300 and 320 K. This is reasonable and expected.

5.2.2. Nitric Oxide, NO

Equation (5) was fit to the $u^2(T, p)$ surface for nitric oxide using the HCLJ model. The resulting fitted four parameters, σ, a, ε/k_B, and ν_{123}/k_B are given in Table IV. The fit had 154 degrees of freedom, ν, and χ^2/ν was 3.98. The data on the 200 K isotherm above 400 kPa had to be excluded from the fit, as systematic deviations showed that a contribution from $D(T)$ was required in this range of density. When the $u^2(T, p)$ data set was fit with only $B(T)$, large systematic deviations are observed indicating $C(T)$ is required. These deviations are larger in the HCLJ model than in the HCSW model. The HCLJ is a more realistic representation of intermolecular interactions, making it less likely that contributions from $C(T)$ end up in the fitted value of $B(T)$. The HCSW and HCLJ models for NO use four parameters, and the HCSW fit is statistically superior, and would provide superior densities over the experimental temperature range. However, the HCLJ, which more accurately represents the intermolecular interactions, will have more accurate values for the actual $B(T)$ and $C(T)$, and will extrapolate better outside of the experimental temperature range.

5.2.3. Interpolation Scheme

The computation of the second and third virial coefficients and their temperature derivatives from Eqs. (10) and (11) using the parameters in Table IV is a numerically intensive process and is not convenient for repetitive calculations. Again, following the lead of Trusler [25], we provide a look-up table for the second and third virial coefficients and their first two derivatives, to allow for interpolation. In the look-up table, a substitution of variables has been performed, such that temperature is presented as reduced reciprocal temperature $\tau = \varepsilon/(k_B T)$ where $T\frac{dB}{dT} = -\tau\frac{dB}{d\tau}$ and $T^2\frac{d^2B}{dT^2} = \tau^2\frac{d^2B}{d\tau^2} + 2\tau\frac{dB}{d\tau}$. In Tables V and VI the virial coefficients are also presented in reduced (dimensionless) form where $B^*(T) = B(T)/b_0$ and $C^*(T) = C(T)/b_0^2$ where $b_0 = 2\pi N_A \sigma^3/3$. Tables V and VI provide reduced temperatures between 0.3 and 4.0 which correspond to approximately 91 to

Table V. Nitrous Oxide HCLJ Reduced Virial Coefficients, where $\tau = \varepsilon/k_B T$ and $\varepsilon/k_B = 446.77$ K and $B^*(T) = B(T)/(b_0)$ and $C^*(T) = C(T)/(b_0)^2$ where $b_0 = \frac{2}{3}\pi N_A \sigma^3$, $\sigma = 0.3595$ nm, and $b_0 = 585.976$ mol·cm^{-3} (Numbers in parentheses are the exponents)

τ	$B(\tau)^*$	$\frac{\partial B(\tau)^*}{\partial \tau}$	$\frac{\partial^2 B(\tau)^*}{\partial \tau^2}$	$\frac{\partial^3 B(\tau)^*}{\partial \tau^3}$	$C(\tau)^*$	$\frac{\partial C(\tau)^*}{\partial \tau}$	$\frac{\partial^2 C(\tau)^*}{\partial \tau^2}$	$\frac{\partial^3 C(\tau)^*}{\partial \tau^3}$
0.3	5.0077(−2)	−2.3922(−1)	−2.7408(−1)	8.3789(−1)	7.5260(−3)	1.6235(−3)	2.2265(−2)	1.9269(−1)
0.4	2.4892(−2)	−2.6367(−1)	−2.2407(−1)	2.6929(−1)	7.8261(−3)	4.5953(−3)	3.5448(−2)	8.7010(−2)
0.5	−2.5605(−3)	−2.8515(−1)	−2.0889(−1)	6.3716(−2)	8.4749(−3)	8.4770(−3)	4.1313(−2)	3.4098(−2)
0.6	−3.2114(−2)	−3.0590(−1)	−2.0782(−1)	−3.1962(−2)	9.5331(−3)	1.2708(−2)	4.2610(−2)	−7.8399(−3)
0.7	−6.3751(−2)	−3.2694(−1)	−2.1394(−1)	−8.6220(−2)	1.1014(−2)	1.6858(−2)	3.9633(−2)	−5.2951(−2)
0.8	−9.7531(−2)	−3.4884(−1)	−2.2448(−1)	−1.2268(−1)	1.2887(−2)	2.0469(−2)	3.1656(−2)	−1.0894(−1)
0.9	−1.3356(−1)	−3.7195(−1)	−2.3821(−1)	−1.5097(−1)	1.5071(−2)	2.2976(−2)	1.7269(−2)	−1.8223(−1)
1.0	−1.7197(−1)	−3.9657(−1)	−2.5456(−1)	−1.7554(−1)	1.7421(−2)	2.3641(−2)	−5.5947(−3)	−2.7971(−1)
1.1	−2.1293(−1)	−4.2294(−1)	−2.7327(−1)	−1.9868(−1)	1.9705(−2)	2.1481(−2)	−3.9756(−2)	−4.0972(−1)
1.2	−2.5662(−1)	−4.5130(−1)	−2.9429(−1)	−2.2168(−1)	2.1580(−2)	1.5189(−2)	−8.8970(−2)	−5.8275(−1)
1.3	−3.0326(−1)	−4.8187(−1)	−3.1763(−1)	−2.4536(−1)	2.2548(−2)	3.0225(−3)	−1.5818(−1)	−8.1224(−1)
1.4	−3.5308(−1)	−5.1490(−1)	−3.4340(−1)	−2.7028(−1)	2.1912(−2)	−1.7328(−2)	−2.5387(−1)	−1.1155
1.5	−4.0633(−1)	−5.5064(−1)	−3.7174(−1)	−2.9686(−1)	1.8709(−2)	−4.8913(−2)	−3.8449(−1)	−1.5150
1.6	−4.6331(−1)	−5.8934(−1)	−4.0284(−1)	−3.2546(−1)	1.1623(−2)	−9.5752(−2)	−5.6103(−1)	−2.0396
1.7	−5.2431(−1)	−6.3131(−1)	−4.3691(−1)	−3.5641(−1)	−1.1241(−3)	−1.6312(−1)	−7.9782(−1)	−2.7268
1.8	−5.8969(−1)	−6.7683(−1)	−4.7421(−1)	−3.9004(−1)	−2.1914(−2)	−2.5794(−1)	−1.1134	−3.6251
1.9	−6.5981(−1)	−7.2627(−1)	−5.1502(−1)	−4.2665(−1)	−5.3924(−2)	−3.8923(−1)	−1.5319	−4.7971
2.0	−7.3508(−1)	−7.7997(−1)	−5.5965(−1)	−4.6659(−1)	−1.0137(−1)	−5.6879(−1)	−2.0846	−6.3239
2.1	−8.1596(−1)	−8.3834(−1)	−6.0846(−1)	−5.1021(−1)	−1.6980(−1)	−8.1197(−1)	−2.8120	−8.3105
2.2	−9.0292(−1)	−9.0181(−1)	−6.6183(−1)	−5.5789(−1)	−2.6654(−1)	−1.1387	−3.7665	−1.0892(1)
2.3	−9.9651(−1)	−9.7087(−1)	−7.2019(−1)	−6.1004(−1)	−4.0119(−1)	−1.5751	−5.0161	−1.4245(1)
2.4	−1.0973	−1.0460	−7.8400(−1)	−6.6711(−1)	−5.8632(−1)	−2.1547	−6.6488	−1.8596(1)
2.5	−1.2059	−1.1279	−8.5379(−1)	−7.2958(−1)	−8.3835(−1)	−2.9214	−8.7783	−2.4239(1)
2.6	−1.3231	−1.2170	−9.3012(−1)	−7.9800(−1)	−1.1787	−3.9318	−1.1552(1)	−3.1555(1)
2.7	−1.4496	−1.3141	−1.0136	−8.7293(−1)	−1.6353	−5.2596	−1.5161(1)	−4.1036(1)
2.8	−1.5862	−1.4200	−1.1049	−9.5503(−1)	−2.2443	−7.0001	−1.9853(1)	−5.3322(1)
2.9	−1.7339	−1.5354	−1.2049	−1.0450	−3.0531	−9.2768	−2.5947(1)	−6.9240(1)
3.0	−1.8937	−1.6613	−1.3142	−1.1436	−4.1229	−1.2250(1)	−3.3857(1)	−8.9862(1)
3.1	−2.0666	−1.7986	−1.4339	−1.2517	−5.5331	−1.6127(1)	−4.4122(1)	−1.1658(2)
3.2	−2.2538	−1.9484	−1.5649	−1.3702	−7.3872	−2.1176(1)	−5.7436(1)	−1.5120(2)
3.3	−2.4567	−2.1120	−1.7083	−1.5001	−9.8188	−2.7745(1)	−7.4702(1)	−1.9606(2)
3.4	−2.6767	−2.2906	−1.8653	−1.6425	−1.3002(1)	−3.6286(1)	−9.7089(1)	−2.5419(2)
3.5	−2.9154	−2.4856	−2.0373	−1.7988	−1.7161(1)	−4.7384(1)	−1.2611(2)	−3.2956(2)
3.6	−3.1744	−2.6986	−2.2256	−1.9701	−2.2589(1)	−6.1795(1)	−1.6374(2)	−4.2729(2)
3.7	−3.4557	−2.9313	−2.4319	−2.1581	−2.9663(1)	−8.0504(1)	−2.1254(2)	−5.5404(2)
3.8	−3.7614	−3.1856	−2.6578	−2.3643	−3.8875(1)	−1.0478(2)	−2.7581(2)	−7.1850(2)
3.9	−4.0936	−3.4636	−2.9054	−2.5905	−5.0860(1)	−1.3629(2)	−3.5787(2)	−9.3193(2)
4.0	−4.4550	−3.7675	−3.1767	−2.8388	−6.6444(1)	−1.7717(2)	−4.6431(2)	−1.2090(3)

Table VI. Nitric Oxide HCLJ Reduced Virial Coefficients, where $\tau = \varepsilon/k_B T$ and $\varepsilon/k_B = 323.677$ K and $B^*(T) = B(T)/(b_0)$ and $C^*(T) = C(T)/(b_0)^2$ where $b_0 = \frac{2}{3}\pi N_A \sigma^3$, $\sigma = 0.3075$ nm, and $b_0 = 366.7307$ mol·cm^3
(Numbers in parentheses are the exponents)

τ	$B(\tau)^*$	$\frac{\partial B(\tau)^*}{\partial \tau}$	$\frac{\partial^2 B(\tau)^*}{\partial \tau^2}$	$\frac{\partial^3 B(\tau)^*}{\partial \tau^3}$	$C(\tau)^*$	$\frac{\partial C(\tau)^*}{\partial \tau}$	$\frac{\partial^2 C(\tau)^*}{\partial \tau^2}$	$\frac{\partial^3 C(\tau)^*}{\partial \tau^3}$
0.3	8.0016(−2)	−3.8223(−1)	−4.3793(−1)	1.3388	1.9215(−2)	4.1451(−3)	5.6845(−2)	4.9196(−1)
0.4	3.9774(−2)	−4.2129(−1)	−3.5803(−1)	4.3028(−1)	1.9981(−2)	1.1732(−2)	9.0502(−2)	2.2214(−1)
0.5	−4.0913(−3)	−4.5562(−1)	−3.3377(−1)	1.0181(−1)	2.1637(−2)	2.1643(−2)	1.0548(−1)	8.7055(−2)
0.6	−5.1312(−2)	−4.8878(−1)	−3.3206(−1)	−5.1070(−2)	2.4339(−2)	3.2444(−2)	1.0879(−1)	−2.0016(−2)
0.7	−1.0186(−1)	−5.2240(−1)	−3.4185(−1)	−1.3777(−1)	2.8119(−2)	4.3039(−2)	1.0119(−1)	−1.3519(−1)
0.8	−1.5584(−1)	−5.5738(−1)	−3.5869(−1)	−1.9602(−1)	3.2901(−2)	5.2258(−2)	8.0821(−2)	−2.7814(−1)
0.9	−2.1341(−1)	−5.9431(−1)	−3.8062(−1)	−2.4122(−1)	3.8477(−2)	5.8659(−2)	4.4089(−2)	−4.6525(−1)
1.0	−2.7478(−1)	−6.3365(−1)	−4.0674(−1)	−2.8048(−1)	4.4477(−2)	6.0357(−2)	−1.4284(−2)	−7.1413(−1)
1.1	−3.4023(−1)	−6.7579(−1)	−4.3665(−1)	−3.1746(−1)	5.0309(−2)	5.4844(−2)	−1.0150(−1)	−1.0461
1.2	−4.1004(−1)	−7.2110(−1)	−4.7022(−1)	−3.5421(−1)	5.5095(−2)	3.8779(−2)	−2.2715(−1)	−1.4878
1.3	−4.8457(−1)	−7.6995(−1)	−5.0752(−1)	−3.9205(−1)	5.7567(−2)	7.7168(−3)	−4.0385(−1)	−2.0737
1.4	−5.6417(−1)	−8.2273(−1)	−5.4870(−1)	−4.3186(−1)	5.5944(−2)	−4.4239(−2)	−6.4816(−1)	−2.8480
1.5	−6.4926(−1)	−8.7983(−1)	−5.9399(−1)	−4.7433(−1)	4.7766(−2)	−1.2488(−1)	−9.8163(−1)	−3.8679
1.6	−7.4029(−1)	−9.4168(−1)	−6.4367(−1)	−5.2003(−1)	2.9674(−2)	−2.4446(−1)	−1.4324	−5.2073
1.7	−8.3776(−1)	−1.0087	−6.9812(−1)	−5.6949(−1)	−2.8698(−3)	−4.1647(−1)	−2.0369	−6.9618
1.8	−9.4223(−1)	−1.0815	−7.5772(−1)	−6.2321(−1)	−5.5949(−2)	−6.5853(−1)	−2.8426	−9.2552
1.9	−1.0543	−1.1605	−8.2292(−1)	−6.8172(−1)	−1.3767(−1)	−9.9373(−1)	−3.9112	−1.2247(1)
2.0	−1.1745	−1.2463	−8.9424(−1)	−7.4554(−1)	−2.5879(−1)	−1.4522	−5.3223	−1.6146(1)
2.1	−1.3038	−1.3395	−9.7222(−1)	−8.1523(−1)	−4.3351(−1)	−2.0730	−7.1793	−2.1217(1)
2.2	−1.4427	−1.4409	−1.0575	−8.9142(−1)	−6.8050(−1)	−2.9073	−9.6163	−2.7809(1)
2.3	−1.5923	−1.5513	−1.1507	−9.7474(−1)	−1.0243	−4.0213	−1.2807(1)	−3.6369(1)
2.4	−1.7533	−1.6714	−1.2527	−1.0659	−1.4969	−5.5012	−1.6975(1)	−4.7477(1)
2.5	−1.9269	−1.8021	−1.3642	−1.1658	−2.1404	−7.4585	−2.2412(1)	−6.1884(1)
2.6	−2.1141	−1.9446	−1.4862	−1.2751	−3.0093	−1.0038(1)	−2.9494(1)	−8.0562(1)
2.7	−2.3162	−2.0998	−1.6196	−1.3948	−4.1750	−1.3428(1)	−3.8708(1)	−1.0477(2)
2.8	−2.5345	−2.2689	−1.7655	−1.5260	−5.7300	−1.7872(1)	−5.0686(1)	−1.3614(2)
2.9	−2.7705	−2.4533	−1.9252	−1.6697	−7.7949	−2.3684(1)	−6.6244(1)	−1.7678(2)
3.0	−3.0258	−2.6545	−2.0999	−1.8273	−1.0526(1)	−3.1275(1)	−8.6440(1)	−2.2943(2)
3.1	−3.3020	−2.8739	−2.2912	−2.0000	−1.4127(1)	−4.1172(1)	−1.1265(2)	−2.9764(2)
3.2	−3.6012	−3.1133	−2.5005	−2.1893	−1.8860(1)	−5.4063(1)	−1.4664(2)	−3.8602(2)
3.3	−3.9254	−3.3746	−2.7296	−2.3969	−2.5068(1)	−7.0836(1)	−1.9072(2)	−5.0055(2)
3.4	−4.2769	−3.6599	−2.9805	−2.6245	−3.3195(1)	−9.2642(1)	−2.4788(2)	−6.4898(2)
3.5	−4.6583	−3.9715	−3.2553	−2.8741	−4.3814(1)	−1.2097(2)	−3.2198(2)	−8.4140(2)
3.6	−5.0722	−4.3119	−3.5561	−3.1479	−5.7671(1)	−1.5777(2)	−4.1805(2)	−1.0909(3)
3.7	−5.5217	−4.6837	−3.8857	−3.4483	−7.5732(1)	−2.0553(2)	−5.4262(2)	−1.4145(3)
3.8	−6.0101	−5.0901	−4.2468	−3.7778	−9.9251(1)	−2.6752(2)	−7.0416(2)	−1.8344(3)
3.9	−6.5410	−5.5342	−4.6423	−4.1392	−1.2985(2)	−3.4796(2)	−9.1366(2)	−2.3793(3)
4.0	−7.1183	−6.0198	−5.0758	−4.5359	−1.6964(2)	−4.5233(2)	−1.1854(3)	−3.0867(3)

1222 K for NO and 111 to 1490 K for NO_2. These ranges greatly exceed our experimental temperature ranges; however, they are reasonable extrapolations based on our experience with CF_4 and C_2F_6 and Trusler's experience with C_3H_8.

6. DISCUSSION

Figures 4 and 5 compare the second and third virial coefficients for each gas for each model, and include any previously published data. Figure 4 (top) shows the second virial coefficient for N_2O, and that the values for $B(T)$ from the HCSW and HCLJ models are indistinguishable except near 200 K. Dymond and Smith [30] observed that there are a number of discrepancies in the older reported values of the second virial coefficient of N_2O, but since 1960 they are in good agreement. They provide recommended smoothed values with uncertainty levels from 240 to 400 K. Our current results agree with their recommended values to within

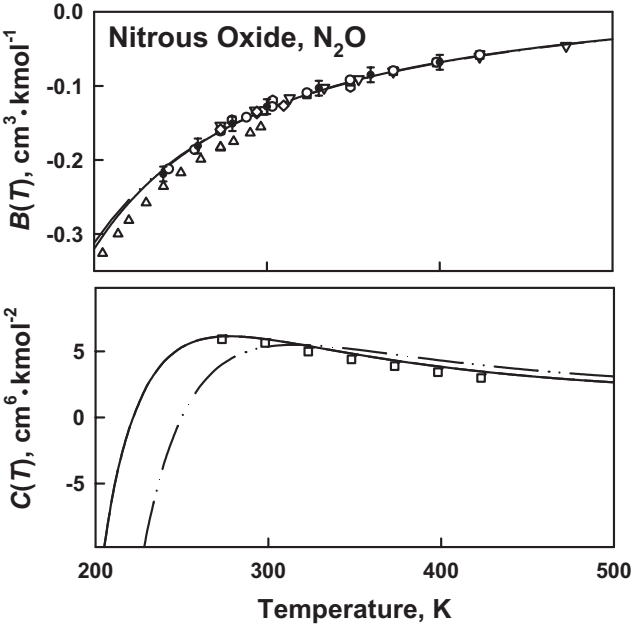

Fig. 4. Virial coefficients for N_2O: (——) HCLJ; (–···–) HCSW; (○) Couch et al. [31]; (□) Schamp et al. [32]; (△) Johnston and Weimer [34]; (▽) Bousheri et al. [15]; (◇) Cawood and Patterson [35]; (⬡) Kirouac and Bose [33]; and (●) smoothed values of Dymond and Smith [30].

these uncertainty levels. The results of Couch et al. [31], Schamp et al. [32], and Kirouac and Bose [33] were published after 1960 and agree with the present results. Johnston and Weimer [34] results from 1934 extend down to 200 K, but appear to be low, and Cawood and Patterson [35] results from 1937 appear slightly high. Boushehri et al. [15] in 1987 predicted values for $B(T)$ from a corresponding states theory. These extend to higher temperatures, and agree with our extrapolated values. Figure 4 (lower) shows the third virial coefficient, $C(T)$ for N_2O. Only Schamp et al. [32] have previously reported $C(T)$ results. These results agree with ours, particularly for the HCLJ model. The HCSW and HCLJ models agree above room temperature, but at the lower temperatures the HCSW goes negative before the HCLJ model. At the lower temperatures $B(T)$ for the HCSW is larger than for the HCLJ, showing how the HCSW $C(T)$ compensates. The $B(T)$ and $C(T)$ in the HCSW model are not coupled, each having three independent variables, while the HCLJ model uses the same "potential" for both $B(T)$ and $C(T)$.

Figure 5 (top) shows the second virial coefficient for NO; the values for $B(T)$ from the HCSW and HCLJ models are indistinguishable on this

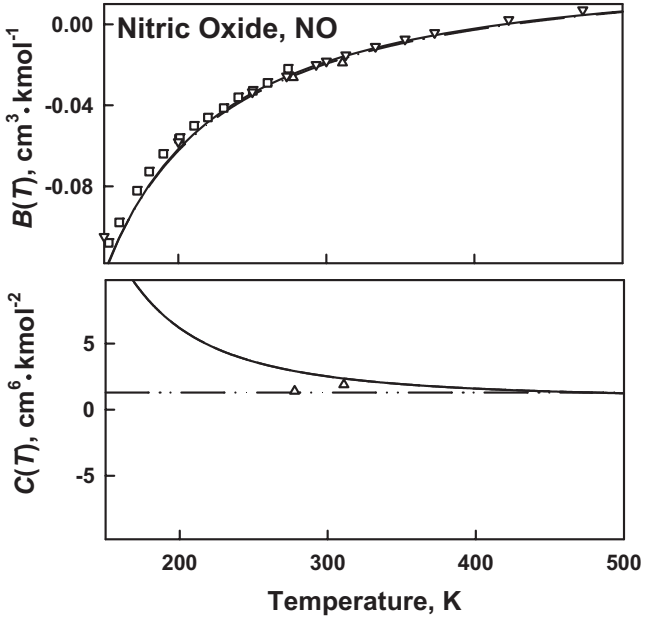

Fig. 5. Virial Coefficients for NO: (——) HCLJ; (–···–) HCSW; (□) Johnston and Weimer [34]; (△) Golding and Sage [36]; (▽) Bousheri et al. [15].

scale. Johnston and Weimer in 1934 [34] reported values for $B(T)$ from 120 to 274 K; for N_2O their results were consistently too low, and for NO they are consistently too high. Golding and Sage [36] in 1951 reported two values at 277.6 and 310.9 K, which agree with our current results. No experimental results for $B(T)$ for NO have been published since 1951; however, Boushehri et al. [15] also predicted values for $B(T)$ for NO from a corresponding states theory. Their predicted values appear good at room temperature, but too high above and below room temperature. Golding and Sage [36] provide the only reported values for $C(T)$. Their results agree with both the HCLJ and the constant HCSW values over the limited temperature range.

REFERENCES

1. K. A. Gillis and M. R. Moldover, *Int. J. Thermophys.* **17**:1305 (1996).
2. J. F. Mathews, *Chem. Rev.* **72**:71 (1972).
3. J. J. Hurly, *Int. J. Thermophys.* **20**:455 (1999).
4. K. A. Gillis, *Int. J. Thermophys.* **15**:821 (1994).
5. K. A. Gillis, A. R. H. Goodwin, and M. R. Moldover, *Rev. Sci. Instrum.* **62**:2213 (1991).
6. J. J. Hurly, *Int. J. Thermophys.* **23**:455 (2002).
7. J. J. Hurly, *Int. J. Thermophys.* **23**:667 (2002).
8. J. J. Hurly, *Int. J. Thermophys.* **21**:805 (2000).
9. J. J. Hurly, *Int. J. Thermophys.* **21**:185 (2000).
10. D. R. Stull, *Ind. Eng. Chem.* **39**:517 (1947).
11. E. F. Westrum, Jr., D. R. Stull, and G. C. Sinke, in *The Chemical Thermodynamics of Organic Compounds* (Wiley, New York, 1969).
12. S. A. Klein, M. O. McLinden, and A. Laesecke, *Int. J. Refrig.* **20**:208 (1997).
13. M. O. McLinden, S. A. Klein, and R. A. Perkins, *Int. J. Refrig.* **23**:43 (2000).
14. L. Riedel, *Chem. Ing. Tech.* **26**:83 (1954).
15. A. Bousheri, J. Bzowski, J. Kestin, and E. A. Mason, *J. Phys. Chem. Ref. Data* **16**:445 (1987).
16. H. L. Johnston and E. R. Grilly, *J. Chem. Phys.* **14**:323 (1946).
17. M. R. Moldover, J. P. M. Trusler, T. J. Edwards, J. B. Mehl, and R. S. Davis, *Phys. Rev. Lett.* **60**:249 (1988); M. R. Moldover, J. P. M. Trusler, T. J. Edwards, J. B. Mehl, and R. S. Davis, *J. Res. Natl. Bur. Stand.* **93**:85 (1988).
18. M. W. Chase, Jr., in *JANAF Thermochemical Tables, 4th Ed., NSRDS-NBS 37* (U.S. Department of Commerce, Washington, D.C., 1998).
19. R. H. Gillette and E. H. Eyster, *Phys. Rev.* **56**:1113 (1939).
20. W. Braker and A. L. Mossman, in *Matheson Gas Data Book, 6th Ed.* (Matheson Company, Inc., Lyndhurst, New Jersey, 1980).
21. E. F. Westrum, Jr., D. R. Stull, and G. C. Sinke, in *The Chemical Thermodynamics of Organic Compounds* (Wiley, New York, 1969).
22. Y. S. Touloukian, in *Thermophysical Properties of Matter* (IFI/Plenum, New York, 1970).
23. D. D. Wagman, R. H. Schumm, V. B. Parker, I. Halow, W. H. Evans, and S. M. Bailey, in *Selected Values of Chemical Thermodynamic Properties, NBS Tech. Note 270–3* (National Bureau of Standards, Washington, D.C., 1968).

24. T. Kihara, *Rev. Mod. Phys.* **25**:831 (1953).
25. J. P. M. Trusler, *Int. J. Thermophys.* **18**:635 (1997).
26. B. M. Axilrod and E. J. Teller, *J. Chem. Phys.* **11**:299 (1943).
27. E. A. Mason and T. H. Spurling, in *The Virial Equation of State* (Pergamon Press, Oxford, 1969).
28. R. J. Dulla, J. S. Rowlinson, and W. R. Smith, *Mol. Phys.* **21**:229 (1971).
29. R. F. Boisvert, S. E. Howe, D. K. Kahaner, and J. L. Springmann, *The Guide to Available Mathematical Software*, NISTIR 90-4237 (1990).
30. J. H. Dymond and E. B. Smith, in *The Virial Coefficients of Pure Gases and Mixtures* (Oxford University Press, New York, 1980).
31. E. J. Couch, L. J. Hirth, and K. A. Kobe, *J. Chem. Eng. Data* **6**:229 (1961).
32. H. W. Schamp, E. A. Mason, and K. Su, *Phys. Fluids* **5**:796 (1962).
33. S. Kirouac and T. K. Bose, *J. Chem. Phys.* **59**:3043 (1973).
34. H. L. Johnston and H. R. Weimer *J. Am. Chem. Soc.* **56**:625 (1934).
35. W. Cawood and J. S. Patterson, *J. Chem. Soc.* 619 (1933); *Philos. Trans. Roy. Soc. Ser. A* **236**:77 (1937).
36. B. H. Golding and B. H. Sage, *Ind. Eng. Chem. Ind. Edn.* **43**:160 (1951).